# The Influence of Antenna Pattern on Faraday Rotation in Remote Sensing at L-band

David M. Le Vine
Goddard Space Flight Center, Greenbelt, MD 20771

S. Daniel Jacob
Goddard Earth Science and Technology Center, Baltimore, Maryland 21250

## Popular Summary

Faraday rotation is a change in the polarization vector of electromagnetic radiation that occurs as the waves propagate from the Earth surface through the ionosphere to a spaceborne sensor. This change can cause errors in monitoring parameters at the surface such as soil moisture and sea surface salinity and it is an important consideration for radiometers on future missions in space such as NASA's Aquarius mission and ESA's SMOS mission. Two prominent strategies for compensating for Faraday rotation are using a sum of the signal at two polarizations and using the correlation between the signals at the two polarizations. These strategies work for an idealized antenna. This paper evaluates the strategies in the context of realistic antennas such as will be built for the Aquarius radiometer. Realistic antennas will make small differences that need to be included in planning for retrieval algorithms in future missions.

The Influence of Antenna Pattern on Faraday Rotation in Remote Sensing at L-band

David M. Le Vine
Goddard Space Flight Center, Greenbelt, MD 20771

S. Daniel Jacob
Goddard Earth Science and Technology Center, Baltimore, Maryland 21250

**Abstract**

The influence of the pattern of the receive antenna on Faraday rotation is examined in the context of passive remote sensing of soil moisture and ocean salinity at L-band. Faraday rotation is an important consideration for radiometers on future missions in space such as SMOS and Aquarius. Using the radiometer on Aquarius as an example, it is shown that while I = Tv + Th is independent of Faraday rotation to first order, it has rotation dependence when realistic antenna patterns are included in the analysis. Also, it is shown that using the 3rd Stokes parameter to measure the rotation angle can yield a result biased by as much as one degree by purely geometrical issues associated with the finite width of the main beam.

## I. Introduction

Faraday rotation is a change in the polarization vector that occurs as electromagnetic waves propagate through the ionosphere. The magnitude of the change varies as $1/(\text{frequency})^2$ and is an important consideration for remote sensing at the low frequency end of the microwave spectrum. For example, at L-band (1.4 GHz) where remote sensing of soil moisture and sea surface salinity is performed, the rotation of the polarization vector can range from a few degrees to more than 15 degrees depending on viewing angle and the solar cycle (Le Vine and Abraham, 2002). The corresponding change in apparent brightness temperature can be several Kelvin and is an important issue for missions such as SMOS (Kerr et al, 2000, 2001) and Aquarius (Le Vine et al, 2006, 2007) which will be launched soon to measure soil moisture and sea surface salinity at L-band.

Unfortunately, current models for the ionosphere are often not sufficiently accurate to make corrections (Abraham and Le Vine, 2001). This is especially true in the case of sea surface salinity which requires high accuracy and measurements over the oceans (Le Vine et al, 2006; Lagerloef, Swift and Le Vine, 1995) where data on the ionosphere is sparse.

Among the strategies adopted to compensate for Faraday rotation is use the first Stokes parameter, I = Tv + Th. In the ideal case when the antenna patterns for the two polarizations are identical and there is no cross-polarization coupling, I is independent of

Faraday rotation. It is also independent of other rotations such as errors in the antenna polarization clocking angle.

Another strategy is to measure the third Stokes parameter TU (see below Equation 5 for a definition). One can show that the ratio of TU to the second Stokes vector, Q = Tv – Th, is proportional to the tangent of twice the angle of Faraday rotation. This was recognized by S. Yueh who described how TU and Q could be used to measure the Faraday rotation (Yueh, 2001).

Both of these strategies work in the case of narrow beam antennas with no cross-polarization coupling. However, at L-band antennas in space tend to have large footprints (e.g. 100 km diameter for Aquarius) and small but not negligible cross-polarization coupling. The purpose of this paper is to examine the performance of these two approaches when used with antennas with realistic patterns. Of concern are the effect of cross-pol coupling, mismatch of the patterns for the two polarizations and the effect of changes in the orientation of the polarization vectors at the surface with respect to boresight over the footprint of the antenna beam. For example, cross-polarization coupling can introduce a dependence on Faraday rotation in the sum I = Tv + Th and also introduce a bias in the estimate of the angle of Faraday rotation obtained from Q and TU. In the sections to follow, expressions for I, Q and TU are derived for a general antenna and examined in special cases. Then, to get realistic estimates of the magnitude of the effects to be expected in the general case, the antennas for the Aquarius radiometer are used to generate numerical results.

## II. Antenna Temperature: General Case

Consider a dual polarized antenna with its two polarization ports, **v** and **h**, arranged so that at boresight the directions correspond to the conventional definitions at the surface:

$$\mathbf{h} = (\mathbf{k} \times \mathbf{n}) / |\mathbf{k} \times \mathbf{n}| \quad (1)$$

$$\mathbf{v} = \mathbf{h} \times \mathbf{k}$$

where **n** is a vector normal to the surface and **k** is the direction of propagation from the surface toward the antenna. Let the antenna "voltage" pattern at each port be:

$$G_h = g_{hh}\,\varepsilon_1 + g_{hv}\,\varepsilon_2 \quad (2)$$

$$G_v = g_{vv}\,\varepsilon_2 + g_{vh}\,\varepsilon_1$$

where the $g_{ij}$ are complex and the $\varepsilon_i$ are unit vectors defined by Ludwig (1973) to indicate the directions of co-polarization and cross-polarization. Assume a local coordinate system at the antenna with unit vectors (**x**,**y**,**z**), and let the z-axis be along the boresight direction (pointing to the surface) and let the x-axis be aligned with the direction of vertical polarization, **v**, at the surface. Then, one has (Lugwig, 1973):

$$\boldsymbol{\varepsilon_1} = [1 + \cos^2\varphi\,(\cos\theta - 1)]\,\mathbf{x} + (\cos\theta - 1)\sin\varphi\cos\varphi\;\mathbf{y} - \sin\theta\cos\varphi\,\mathbf{z}$$

$$\boldsymbol{\varepsilon_2} = (\cos\theta - 1)\sin\varphi\cos\varphi\;\mathbf{x} + [1 + \sin^2\varphi\,(\cos\theta - 1)]\,\mathbf{y} - \sin\theta\sin\varphi\,\mathbf{z} \qquad (3)$$

The antenna output, the antenna temperature $T_A$, can be written in the form (Camps et al, 2005):

$$T_A = \int G(\Omega)\, R(\Omega)\, T_B(\Omega)\, d\Omega \qquad (4)$$

where $T_B$ is the "modified" Stokes vector, in units of brightness temperature, evaluated at the surface:

$$T_B = \begin{matrix} Tv \\ Th \\ T3 \\ T4 \end{matrix} \qquad (5)$$

where T3 = TU = $2\,\alpha$ Re<Eh*Ev> and T4 = TV = $2\,\alpha$ Im <Eh*Ev> and the coefficient of proportionality is $\alpha = \lambda^2/(\eta k)$ where $\eta = \sqrt{\mu/\varepsilon}$ is the intrinsic impedance of the medium, k is the Boltzmann constant, and <> indicates the expected value.

In Equation 4, R is a "rotation" matrix:

$$R = \begin{matrix} \cos^2\varphi_c & \sin^2\varphi_c & 0.5\sin 2\varphi_c & 0 \\ \sin^2\varphi_c & \cos^2\varphi_c & -0.5\sin 2\varphi_c & 0 \\ -\sin 2\varphi_c & \sin 2\varphi_c & \cos 2\varphi_c & 0 \\ 0 & 0 & 0 & 1 \end{matrix} \qquad (6)$$

and G in Equation 4 is an antenna pattern matrix:

$$G = \begin{matrix} |g_{vv}P|^2 & |g_{vh}P|^2 & \mathrm{Re}(g_{vv}\, g_{vh}^*) & -\mathrm{Im}(g_{vv} g_{vh}^*) \\ |g_{hv}P|^2 & |g_{hh}P|^2 & \mathrm{Re}(g_{hh}^*\, g_{hv}) & -\mathrm{Im}(g_{hh}^*\, g_{hv}) \\ 2\mathrm{Re}(g_{vv}\, g_{hv}^*) & 2\mathrm{Re}(g_{hh}^*\, g_{vh}) & \mathrm{Re}(g_{vv} g_{hh}^* + g_{vh} g_{hv}^*) & -\mathrm{Im}(g_{vv} g_{hh}^* + g_{vh} g_{hv}^*) \\ 2\mathrm{Im}(g_{vv}\, g_{hv}^*) & 2\mathrm{Im}(g_{hh}^*\, g_{vh}) & \mathrm{Im}(g_{vv} g_{hh}^* + g_{vh} g_{hv}^*) & \mathrm{Re}(g_{vv} g_{hh}^* - g_{vh} g_{hv}^*) \end{matrix} \qquad (7)$$

The matrix in Equation 7 above appears in scattering theory where the parameters $g_{ij}$ are replaced by scattering coefficients and it is commonly called the "Stokes matrix" (e.g. Fung, 1994; Tsang, Kong and Shin, 1985).

In Equation 6, the angle $\varphi_c = \varphi + \Omega_F$ where $\Omega_F$ is the Faraday rotation angle (Appendix B, section A) and $\varphi$ is a geometry dependent rotation. The later occurs because the polarization vectors defined on the surface (**h** and **v** in Equation 1) are only aligned with the polarization vectors of the antenna (Equations 3) at boresight. Along other rays from the antenna to the surface, the polarization vectors at the surface are rotated relative to vectors defined in Equation 3 (see Appendix B section B; also Dinnat and Le Vine, 2007). Although not considered here, it is also possible to have a rotation about boresight of the antenna polarization vectors themselves relative to the desired orientation (e.g. a misalignment of the polarization vectors due to mechanical error). This would appear as a constant offset, $\varphi_0$, that would be included in $\varphi_c$.

## III. Special Cases

The matrix operations that result from substituting Equations 5-7 into the integrand of Equation 4 are straight forward but the expressions that result are rather long. The general expressions are given in Appendix A and they will be used for the numerical computations to be discussed below (Section IV). However, in order to gain insight, it is convenient to first look at special cases. In the discussion below, I = Tv + Th and Q = Tv – Th and T3 = 2 α Re<Eh*Ev>. Parameters without primes are measured at the surface. Parameters with primes (i.e. I', Q' and T3 ) have the same definition but are measured at the sensor after propagation through the ionosphere and being weighted by the antenna pattern (Equation 7) but before integration. That is, they are the result of the matrix product $G(\Omega)\, R(\Omega)\, T_B(\Omega)$ in Equation 4.

### A. Ideal Antenna Patterns

The general expressions simplify greatly if one assumes that the antenna patterns for the two polarizations are identical and that there is no cross-polarization coupling. In particular, assume $g_{hh} = g_{vv} = G$ and $g_{hv} = g_{vh} = 0$. In this case, one obtains the conventional results and the first Stokes parameter, I' = Tv' + Th', is independent of Faraday rotation. Combining the first two rows in the integrand in Equation 4, one obtains:

$$I' = G^2\, I \tag{8a}$$

$$Q' = G^2 \cos(2\varphi_c)\, Q + G^2 \cos(2\varphi_c)\, T3 \tag{8b}$$

$$T3 = G^2 \cos(2\varphi_c)\, T3 - G^2 \sin(2\varphi_c)\, Q \tag{8c}$$

where it has been assumed that T4 = 0 at the surface, but T3 ≠ 0 and the primes on the quantities on the left are a reminder that the integration in Equation 4 has not been done.

Notice, that in this case, I' is independent, not only of Faraday rotation, $\Omega_F$, but also of any geometrical effects, $\varphi$. As mentioned above, a non-zero value of $\varphi$ can arise because the polarization vectors at the surface are not aligned with the polarization vectors defined at the antenna ports (Appendix B section B). In the ideal case, the first Stokes parameter has the added advantage of being independent of both, $\varphi$ and $\Omega_F$.

Also, notice that when the third Stokes parameter at the surface, T3, is zero, then the ratio, T3 / Q' is proportional to the tangent of $2\varphi_c$:

$$\varphi_c = 0.5\ \mathrm{Tan}^{-1}(T3 / Q') \tag{9}$$

Yueh (2001) proposed the use of T3 and Q' in this manner to measure Faraday rotation. He discussed the impact on the retrieval when the third Stokes parameter at the surface, T3, is not zero. However, he did not consider the effects of the integration over the footprint (i.e. the integration in Equation 4 over solid angle, $d\Omega$, remains to be performed). For a very narrow antenna pattern, this is not an issue. However, for a broad antenna pattern such as is likely to be the case at L-band for antennas in space (Le Vine et al, 2006), the variation of geometry over the footprint must be taken into account. As will be shown in the examples later, a bias can arise due to non-zero $\varphi$ when this integration is performed.

B. Impact of Cross-Pol Coupling

Let the antenna patterns be identical as in the case above, but in this case assume non-zero cross-polarization coupling. That is, assume $g_{hh} = g_{vv} = G$ as before but instead of zero cross-pol coupling assume $g_{hv} = g_{vh} = g$. In this case, the terms in the integrand in Equation 4 can be written in the form:

$$\begin{aligned} I' &= (G^2 + g^2)\ I - 2\,\mathrm{Re}(Gg^*)\sin(2\varphi_c)\ Q + 2\,\mathrm{Re}(Gg^*)\cos(2\varphi_c)\ T3 \\ Q' &= (G^2 - g^2)\cos(2\varphi_c)\ Q + (G^2 - g^2)\sin(2\varphi_c)\ T3 \\ T3 &= (G^2 + g^2)\cos(2\varphi_c)\ T3 + 2\,\mathrm{Re}(Gg^*)\ I - (G^2 + g^2)\sin(2\varphi_c)\ Q \end{aligned} \tag{10}$$

In most cases g is small and $g^2 << G^2$. Assuming this to be the case and keeping only terms of first order in g, the results simplify to:

$$I' = G^2 I + 2\,\mathrm{Re}(Gg^*)\sin(2\varphi_c)\ Q + 2\,\mathrm{Re}(Gg^*)\cos(2\varphi_c)\ T3 \tag{11a}$$

$$Q' = G^2\cos(2\varphi_c)\ Q + G^2\sin(2\varphi_c)\ T3 \tag{11b}$$

$$T3 = G^2\cos(2\varphi_c)\ T3 + 2\,\mathrm{Re}(Gg^*)\ I - G^2\sin(2\varphi_c)\ Q \tag{11c}$$

Even neglecting T3 which is likely very small at L-band (Yueh, 2000), the first Stokes vector, I', is now no longer independent of either Faraday rotation or of geometry effects,

$\varphi$. Also, now it is coupled to the second Stokes vector, Q, and therefore is likely to be more dependent on local incidence angle, $\theta$, than before. At modest incident angles and flat surfaces with no roughness, I = Tv + Th is almost constant, but Q = Tv - Th increases with incidence angle. In addition, even when T3 = 0, the third Stokes parameter at the sensor, T3 , now is biased relative to its value in the ideal case by the factor 2 Re(Gg*) I. This term is independent of $\varphi_c$. Assuming $g << G$ and $\cos(2\varphi_c) \approx 1$, one can apply Equation 9 to retrieve Faraday rotation, but now the result will be biased by a term which depends on the magnitude of (gI/GQ).

C. Size of the Footprint

The discussion above does not include the effects of the integration in Equation 4 over the antenna pattern. It does apply to an antenna with a narrow beam because in this case, to a first approximation, the integrand can be pulled out of the integral. However, with the relatively broad main beams likely at L-band (Dinnat and Le Vine, 2006) variations over the footprint must be taken into account. Even in the idealized case (Equations 8), I and Q obtained from the apparent antenna temperature, $T_A$, on the left-hand side of Equation 4, can differ from their values at boresight because of variations of the local incidence angle over the footprint. The same is true in the situation described in Equations 11, although more complex because in addition to changes in I and Q with incidence angle, $\varphi_c$ can vary over the footprint. To get an idea of the magnitude of these effects, numerical examples are presented in the following section.

IV. Examples

In order to obtain a more complete picture of how important the size of antenna footprint and presence of cross-polarization coupling are in a realistic case, the integration in Equation 4 has been evaluated using the antenna patterns for the radiometer being developed for the Aquarius instrument (Le Vine et al, 2006, 2007). Aquarius is an L-band microwave instrument being developed to map the salinity field at the surface of the ocean from space. It is part of the Aquarius/SAC-D mission, a partnership between the USA (NASA) and Argentina (CONAE) with launch scheduled in 2009 (Sen, et al, 2006). The Aquarius antenna is a 2.5-m offset parabolic reflector with three feed horns. The three beams are arranged to image in pushbroom fashion with the beams pointed across track, roughly 90 degrees with respect to the spacecraft heading, at look angles of 25.8, 33.8 and 40.3 degrees with respect to the satellite nadir. The resolution of the three radiometer beams ranges from 76 x 94 km for the inner beam to 97 x 157 km for the outer beam and the antennas have a beam width (FWHM) of about 6.5 degrees. The antenna patterns (co-pol and cross-pol) for the horizontally polarized port of the outer beam are shown in Figure 1. The patterns for the other beams are similar (e.g. Dinnat and Le Vine, 2007, Fig 2). These are calculated antenna patterns developed with modern antenna modeling tools and provided by the Aquarius antenna engineering team and have recently been validated with measurements on a scale model (Joe Vecchione, unpublished communication).

Calculations have been made using the antenna patterns described above and the orbit geometry of the Aquarius sensor. Aquarius will be launched into a sun-synchronous orbit at an altitude of 657 km, an inclination of 98 degrees and equatorial crossing times of 6 am (descending) and 6 pm (ascending). The orbit is a 7-day exact repeat orbit. Figure 2a shows the ground track for a representative orbit (bold solid line) and the intersection of the boresight ray with the surface for the three beams (dotted lines). The Aquarius antenna patterns are used for the elements of the matrix G in Equation 7 and the orbit geometry shown in Figure 2 is used to evaluate the elements of the matrix R in Equation 6 and also to determine the brightness temperature vector at the surface, $T_B$. An example of the antenna temperature, Tv, obtained in this manner from Equation 4 is shown in Figure 2b. Values are shown for each of the three beams during one orbit. The horizontal axis (abscissa) is labeled in sample points around the orbit. The calculations are done once each 6 seconds and the results are numbered (1-980) and plotted sequentially as the spacecraft orbits. The large changes in antenna temperature occur at water/land boundaries and are due to large difference in emissivity of land compared to water. The jumps are slightly displaced relative to each other because the beam centers are not co-aligned (see the dotted lines in Figure 2a).

In order to keep the focus on the issue of Faraday rotation, a number of simplifications have been made in the calculations. First of all, it will be assumed that extraterrestrial contributions such as the sun and cosmic background are zero, in which case only the integration over the over the visible disk is relevant. (See Dinnat and Le Vine, 2007 for a discussion of the effect of the integration over the off-earth background.) Second, it is assumed that the surface consists of only water and at a constant temperature (25 C) and a constant salinity (35 psu). This eliminates the jumps and small variations seen in Figure 2a due to land/water crossings and naturally occurring changes in water parameters which otherwise would distract from the issues at hand. Finally, all factors, other than Faraday rotation which normally contribute to the observed antenna temperature (e.g. atmospheric emission and attenuation, reflected radiation from the sun and cosmic background) have been set to zero. With these assumptions, the only contribution other than radiation from the surface is due to Faraday rotation. Faraday rotation is computed using the IRI-2000 to model the ionosphere (Bilitza, 2001) and the International Geomagnetic Reference Field (IGRF) for the Earth magnetic field (Barton, 1997). Details are given in Appendix B.

A. Ideal Case

In the ideal case, the antenna patterns at each polarization are identical and there is no cross-polarization coupling. The integrand in this case is given in Equations 8 and the integration in Equation 4 will be done numerically using the pattern for the H-polarization channel of Aquarius radiometer shown in Figure 1. The co-polarized pattern is used for both the H- and V-polarized channels and the cross-polarization coupling terms ($g_{vh}$ and $g_{hv}$ in Equation 2) are set to zero. The pattern was re-normalized to account for the fact that the integration is only over the visible disk (Le Vine and Dinnat, 2007).

A.1 First Stokes Parameter

As expected fromEquation 8a, the first Stokes parameter, I = Tv + Th, is essentially constant around the orbit and independent of Faraday rotation. However, the value obtained after integration is not exactly the same as the value at boresight. This is shown in Table I which gives the values obtained for the three beams at boresight and after integration. The integrated value differs from its value at boresight the local incidence angle ranges from 0 to about 65 degrees over the visible disk and there is enough energy in the sidelobes of the antenna at the large incidence angles to make a small difference.

Table I
First Stokes Parameter

| Beam | | I = Tv + Th | |
|---|---|---|---|
| | | Integrated | Bore Sight |
| | | | |
| Inner Beam | | 182.6 | 182.4 |
| Middle Beam | | 184.7 | 184.3 |
| Outer Beam | | 188.7 | 187.7 |
| | | | |

A.2 Retrieved Rotation Angle

Figure 3-4 show the angle retrieved using the ratio of the second and third Stokes parameters. In this case the integration in Equation 4 is done as above and the rotation angle is obtained from:

$$\varphi_c = 0.5\ \mathrm{Tan}^{-1}\left( T3_A / Q_A \right) \qquad (13)$$

where the subscript "A" is a reminder that these are the values after integration from the apparent temperature vector, $T_A$. Figure 3 shows the retrieved angle in the case of no Faraday rotation to illustrate the impact of purely geometrical factors. The vertical axis is the retrieved angle and the horizontal axis is labeled in sample points along the orbit: The spacecraft starts on the equator (index "1") and 6 seconds later a second calculation is made (index "2 ), continuing in 6 second steps until the spacecraft rotates one orbit (index "980 ). The three curves show the retrieved angle for the three Aquarius beams. Since the Faraday rotation is zero, the retrieved angle is due entirely variations of the polarization vectors at the surface over the FOV of the antenna relative to their values at boresight. The angle is constant because the geometry changes very little as the spacecraft orbits (there is a small change in altitude). The retrieved angle is different for the three beams because the antenna patterns and boresight direction are different.

Figure 4 shows the angles retrieved using Equation 13 but with Faraday rotation included. In this case, the dominant contribution to $\varphi_c$ is no longer geometry but Faraday rotation in the ionosphere. The shape of the curve reflects changes in the electron density

and magnetic field along the orbit. The ionosphere is the IRI-2000 model for November 14, 2004, a period of low solar activity. Notice the sign change that occurs when the spacecraft crosses the equator (near index 450). This is due to the change in the "dip" angle of the magnetic field relative to the boresight vector (e.g. Le Vine and Abraham, 2000). The dashed line gives the Faraday rotation at boresight as a reference and the solid line is the angle retrieved from Equation 13. The slight difference is primarily due to the geometry effects shown in Figure 3 which are zero at boresight. Faraday rotation depends on the total electron content along the line of sight and the orientation of the line of sight with respect to the local magnetic field. In the case of the three Aquarius beams, the middle beam points slightly aft of across-track and the inner and outer beam point slightly forward. This difference in azimuth accounts for the offset of the middle beam relative to the outer two which is evident, for example, at the beginning of the record.

B. Effect of Cross-Polarization Coupling

Figures 5-7 illustrated the impact of cross-polarization coupling (Equations 11). The calculations are done as above using the pattern for the H-polarized channel of the outer beam used for both polarizations, but in this case with the cross-polarization coupling term included (Figure 1b).

Figure 5-6 show the angle retrieved using Equation 13. Figure 5 shows the case with no Faraday rotation to illustrate the influence of geometric effects on the retrieved angle. Comparing with Figure 3 indicates that the bias is larger in magnitude for the inner and outer beams and somewhat smaller for the middle beam when cross-polarization is included. Figure 6 shows the case with Faraday rotation. Faraday rotation again dominates the retrieved angle, and as before the retrieved value is biased relative to the value at boresight. The behavior is similar to that shown in Figure 4 but with different bias.

Table II shows a comparison of the bias in the cases with cross-polarization coupling (CP) and without cross-polarization coupling (NCP). In the columns labeled, "No Faraday Rotation", theses are the values from Figures 3 and 5. The entries in the columns labeled, "Faraday Rotation", are the mean difference between the retrieved angle and the angle at boresight (difference between the dashed and solid curves in Figures 4 and 6). In the case of the inner and outer beams, the magnitude of geometry-induced bias has increased when cross-polarization coupling is included. But it is slightly smaller for the middle beam. Apparently, this is an indication of the dependence of the bias on the antenna pattern and orientation. Comparing the two columns under "No Faraday Rotation" with their counterparts under "Faraday Rotation", it is clear that the bias relative to the value at boresight is very close to the geometry-induced bias in both cases with and without cross-polarization coupling. The numbers shown in the table are averages over the orbit, but there was very little variation and the RMS value was about the same as the mean value.

Table II
Bias with Cross-Pol Coupling Included

| Beam | No Faraday Rotation | | Faraday Rotation* | |
|---|---|---|---|---|
| | NCP | CP | NCP | CP |
| Inner | -0.346 | -0.903 | -0.358 | -0.910 |
| Middle | 0.436 | 0.340 | 0.423 | 0.332 |
| Outer | -0.161 | -0.399 | -0.188 | -0.426 |

*Mean difference between value at boresight and retrieved value

Figure 7 illustrates the impact of cross-polarization coupling on the first Stokes parameter, I = Tv + Th. It is clear from Equation 11a that when cross-polarization coupling is included, the first Stokes parameter is no longer independent of Faraday rotation. This is illustrated in Figure 7 which shows I for the outer beam obtained by doing the integration in Equation 4 and then adding Tv and Th. The integration is done as above with cross-polarization coupling is included but using the same pattern for both the h-pol and v-pol ports. The dependence on Faraday rotation is clearly evident. Notice the similarity of the shape of the curve with those in Figures 4 and 6 which show the retrieved Faraday rotation angle. The dependence is rather small, with a peak-peak change of about 0.1 K. However, if the goal is to measure sea surface salinity with an accuracy of 0.2 psu, which is the goal of the Aquarius mission (Le Vine et al, 2006), this is a significant variation since the sensitivity at L-band is about 0.5K per psu.

C. General Case

Examples are shown for the general case in Figures 8-9. In this case the calculations are done using Equations A4 with the actual antenna patterns for each polarization and each beam. Cross-polarization coupling is included and the patterns are not identical for each polarization port of the same beam as they were in all the cases above.

C.1. First Stokes Parameter

An example of the first Stokes parameter, I = Tv + Th, in the general case is shown in Figure 8. Examples are shown for the outer beam in the case of low solar activity (LSA) and high solar activity (HSA). The case for low solar activity is the same ionosphere as used in the examples above November 14, 2004), and in this case the dependence on Faraday rotation is about the same as in the special case discussed above in Section B. There is a slight difference in amplitude between the LSA case in Figure 8 and Figure 7 but this is probably a coincidence of the patterns used and the slight mismatch between

the patterns at the two polarization ports which occurs in the general case. In the case of high solar activity the dependence on Faraday rotation is more pronounced. The peak-peak change around the orbit is about 0.1K in the case of LSA and about 0.2 K in the HSA case. This is still a small percentage change. The example suggests that the first Stokes parameter may be a good choice even when slight mismatches in the antenna pattern at each polarization are present. However, as noted above, if accuracy better than 0.1K is required, then using first Stokes parameter to avoid Faraday rotation may not be sufficient. Figure 8 suggests that, in this case, an additional correction for the rotation angle may be needed.

C.2. Retrieved Rotation Angle

Figure 9 shows the angle retrieved using Equation 13 for each beam together with the Faraday rotation at boresight (dashed line). Figure 9a presents the results in the case of low solar activity using the same ionosphere as in the previous examples. Figure 9b is the same calculation but with an ionosphere corresponding to high solar activity. The general features are the same in the two cases, but the scale in Figure 9b is different and corresponds to a much larger Faraday rotation.

Although the biases between the angle at boresight and the retrieved angle are different in the general case compared to either of the special cases above, they are still relatively constant over the orbit. Also, they are about the same in Figures 9a and 9b (high and low solar activity). This is illustrated in Table III which shows the mean value of the difference between the retrieved angle and the value at the beam boresight in the case of high solar activity (HSA) and low solar activity (LSA). The column titled "Mean Bias" is the average value of the difference between the solid and dashed curves in Figure 9 and the column labeled "RMS Bias" is the RMS value of this difference. The "RMS Bias" is

Table III
Bias in the General Case

| Beams | Mean Bias* (degrees) | | RMS Bias (degrees) | |
|---|---|---|---|---|
| | LSA | HSA | LSA | HSA |
| | | | | |
| Inner | 0.827 | 0.833 | 0.024 | 0.050 |
| Middle | -0.730 | -0.688 | 0.057 | 0.138 |
| Outer | 0.341 | 0.401 | 0.067 | 0.170 |

* Mean difference between dashed and solid curve in Figure 8

also equivalent to the difference between the dashed curves Figure 9 and the solid line shifted by the mean value of the bias. This is an indication of how well one could correct

for the bias if one had a reference point some where along the orbit to measure the offset. For example, if the satellite passed over a sounder where an accurate, independent calculation of Faraday rotation could be made and used to remove the bias. For example, assuming such a procedure was used to correct the middle beam, Table III suggests and that error over the orbit would be on the order of 0.14 degrees in the case of high solar activity.

## V. Discussion

In the analysis presented above it was shown that when antenna pattern characteristics such as cross-polarization coupling are included, the first Stokes parameter, I = Tv + Th, is no longer completely independent of Faraday rotation and also that angle obtained from the second and third Stokes parameters, using Equation 13, is biased relative to the Faraday rotation at boresight.

Assuming a well designed antenna with small cross-polarization coupling, the dependence of I on Faraday rotation is of second order (less than 0.1 % in Figure 7). However, even at this level (0.12 K pk-pk) it can be important for the measurement of sea surface salinity where the sensitivity to changes in salinity is on the order of 0.5K/psu. An uncertainty of 0.1K is roughly 0.2 psu which is the measurement goal of the Aquarius mission (Le Vine, et al, 2006; Sen et al, 2006).

Another approach to managing the effect of Faraday rotation is to try to measure the rotation angle. This can be done by measuring the 3$^{rd}$ Stokes parameter and using Equation 13 to retrieve the rotation angle. Two complicating factors are the presence of correlated fields at the surface (Yueh, 20001) and departures of the antenna pattern from ideal. It was shown above that when taking into account realistic antenna patterns, a bias in the retrieved angle occurs. This is due in part to changes in geometry over the footprint of the main beam of the antenna (e.g. Figure 3). Cross-polarization coupling also contributes a bias (e.g. Figure 5). The biases depend on the antenna and its orientation but the examples in Figure 8 indicate that the biases are relatively stable over an orbit. Because of this, it may be possible to correct for the bias by comparing with an independent measurement of Faraday rotation. For example, if the sensor passes over a reference site (e.g. site of an ionospheric sounder) where the true Faraday rotation is known, it might be possible to use this value to correct for the bias. The column labeled RMS Bias in Table III is an indication of how well this might work. It suggests that correction to better than 0.17 degrees might be possible.

Measuring the angle of Faraday rotation is equivalent to measuring the electron content of the ionosphere. For example, see Equation B3 in Appendix B. This could be of particular value over the ocean where soundings to monitor the ionosphere are widely separated. Using the values in Table III as a measure of accuracy and the dynamic range in Figures 9 as an indication of the magnitude of the change, suggests that VTEC could be measured with an accuracy of about 2-3%. For a satellite in low earth orbit and high solar activity this is on the order of 1 TECU (Fig 1 in Le Vine and Abraham, 2002).

VI. References

S. Abraham and D.M. Le Vine, "Evaluation of IRI-95 to Correct Errors Caused by Faraday Rotation in Passive Microwave Remote Sensing from Space," Advances in Space Research, vol 27/1, pp. 153-156, 2001.

C. E. Barton, "International Geomagnetic Reference Field: The seventh generation," J. Geomag. Geoelectr., vol. 49, pp. 123-148, 1997.

D. Bilitza, "International Reference Ionosphere 2000," Radio Science, Vol. 36(2), pp. 261- 265, 2001.

A. Camps, I. Corbella, F. Torres, M. Vall-llossera, and N. Duffo, "Polarimetric Formulation of the Visibility Function Equation Including Cross-Polar Antenna Patterns," IEEE Geoscience and Remote Sensing Letters , vol. 2 , pp. 292-295, 2005

E. Dinnat and D.M. Le Vine, "Effects of the Antenna Aperture on Remote Sensing of Sea Surface Salinity at L-band", IEEE Trans GRS, Special Issue on MicroRad06, accepted for publication, 2007.

A.K. Fung, Microwave Scattering and Emission Models and Their Applications, Artec House, Norwood, MA, 1994 (Section 1.5.1).

G.S.E. Lagerloef, C. Swift and D.M. Le Vine, "Sea Surface Salinity : The Next Remote Sensing Challenge", Oceanography, Vol 8, pp 44-50, 1995.

D.M. Le Vine. G.S.E. Lagerloef, R. Colomb, S. Yueh, F. Pellerano, "Aquarius: An Instrument to Monitor Sea Surface Salinity from Space", IEEE Trans GRS, submitted and revised, 2007

D. Le Vine, G. Lagerloef, F. Pellerano, S . Yueh, and R. Colomb, "Aquarius: A Mission to Monitor Sea Surface Salinity from Space", in Proceedings MicroRad' 06 , (San Juan, Puerto Rico) , 2006.

D. M. Le Vine and S. Abraham, "Faraday Rotation and Passive Microwave Remote Sensing of Soil Moisture from Space," Microw. Radiomet. Remote Sens. Earth's Surf. Atmosphere, pp 89-96, Edited by P. Pampaloni and S. Paloscia, VSP., 2000.

A. Ludwig, "The Definition of Cross Polarization," IEEE Transactions on Antennas and Propagation, vol. 21, pp. 116 119, Jan. 1973.

Y. H. Kerr, Waldteufel P., Wigneron J. P., Martinuzzi J. M., Lazard B., Goutoule J. M. and Lannes A., "The Soil Moisture and Ocean Salinity Mission: An Overview", Microwave Radiometry & Remote Sensing of the Earth's Surface and Atmosphere, VSP, The Netherlands, P. Pampaloni and S. Paloscia, Ed., pp 467-475, 2000.

Y. Kerr et al.: "Soil Moisture Retrieval from Space: The Soil Moisture and Ocean Salinity (SMOS) Mission", IEEE Trans. Geosci. and Remote Sens., Vol. 39 (# 8), August, 2001.

A. Sen, Y. Kim, D. Caruso, G. Lagerloef, R. Colomb, S. Yueh and D. Le Vine, "Aquarius/SAC-D Mission Overview", Proc. SPIE 13th International Symposium on Remote Sensing, Stockholm, Sweden, September 2006.

L. Tsang, J.A. Kong and R. T. Shin, Theory of Microwave Remote Sensing, Wiley and Sons, Inc., 1985 (Section 3.2).

S. Yueh, "Estimates of Faraday Rotation with Passive Microwave Polarimetry for Microwave Remote Sensing of Earth Surfaces", IEEE Trans. Geosci. & Remote Sens., Vol 38 (#5), pp 2434-2438, 2000.

S. H. Yueh, ``Modeling of Wind Direction Signals in Polarimetric Sea Surface Brightness Temperatures," IEEE Transactions on Geoscience and Remote Sensing, vol. 35, no. 6, pp. 1400-1418, 1997.

# Appendix A

## General Case

The objective of this appendix is to provide explicit expressions for the integrand in Equation 4 of the text:

$$T_A = \int G(\Omega)\, R(\Omega)\, T_B(\Omega)\, d\Omega \qquad \text{(A1)}$$

where $T_B$ is the brightness temperature at the surface expressed in form of the modified Stokes vector:

$$T_B = \begin{matrix} Tv \\ Th \\ T3 \\ T4 \end{matrix} \qquad \text{(A2)}$$

where T3 ~ 2 α Re<Eh*Ev> and T4 ~ 2 α Im <Eh*Ev> and the coefficient of proportionality is $\alpha = 1/(\eta k B)$ is defined in the text.

The matrix multiplications are done here in two steps. The first step is to evaluate the matrix product, $T1 = R(\Omega)\, T_B(\Omega)$. The 4 rows of T1 are:

$$\begin{aligned} Tv1 &= \cos^2\varphi_c\, Tv + \sin^2\varphi_c\, Th + 0.5 \sin 2\varphi_c\, T3 \\ Th1 &= \cos^2\varphi_c\, Tv + \sin^2\varphi_c\, Th - 0.5 \sin\varphi_c\, T3 \\ T31 &= -\sin 2\varphi_c\, Tv + \sin 2\varphi_c\, Th + \cos 2\varphi_c\, T3 \\ T41 &= T4 \end{aligned} \qquad \text{(A3)}$$

The second step is to evaluate the matrix product, $T2 = G(\Omega)\, T1(\Omega) = G(\Omega)\, [\, R(\Omega)\, T_B(\Omega)\, ]$. The 4 rows of T2 are the elements of the integrand in Equation A4 above. One obtains:

$$\begin{aligned} Tv2 = {} & |g_{vv}P|^2 (\cos^2\varphi_c\, Tv + \sin^2\varphi_c\, Th + 0.5 \sin 2\varphi_c\, T3) + \\ & |g_{vh}P|^2 (\sin^2\varphi_c\, Tv + \cos^2\varphi_c\, Th - 0.5 \sin\varphi_c\, T3) + \\ & \mathrm{Re}(g_{vv}\, g_{vh}^*) (-\sin 2\varphi_c\, Tv + \sin 2\varphi_c\, Th + \cos 2\varphi_c\, T3) - \\ & \mathrm{Im}(g_{vv}\, g_{vh}^*)\, T4 \end{aligned} \qquad \text{(A4a)}$$

$$\begin{aligned} Th2 = {} & |g_{hv}P|^2 (\cos^2\varphi_c\, Tv + \sin^2\varphi_c\, Th + 0.5 \sin 2\varphi_c\, T3) + \\ & |g_{hh}P|^2 (\sin^2\varphi_c\, Tv + \cos^2\varphi_c\, Th - 0.5 \sin\varphi_c\, T3) + \\ & \mathrm{Re}(g_{hv}\, g_{hh}^*) (-\sin 2\varphi_c\, Tv + \sin 2\varphi_c\, Th + \cos 2\varphi_c\, T3) - \\ & \mathrm{Im}(g_{hv}\, g_{hh}^*)\, T4 \end{aligned} \qquad \text{(A4b)}$$

$$
\begin{aligned}
T32 = \quad & 2\mathrm{Re}(g_{vv}\, g_{hv}^{*})\,(\cos^2\varphi_c\ Tv + \sin^2\varphi_c\ Th + 0.5\sin 2\varphi_c\ T3) + \\
& 2\mathrm{Re}(g_{hh}^{*}\, g_{vh})\,(\sin^2\varphi_c\ Tv + \cos^2\varphi_c\ Th - 0.5\sin\varphi_c\ T3) + \\
& \mathrm{Re}(g_{vv}g_{hh}^{*} + g_{vh}g_{hv}^{*})\,(-\sin 2\varphi_c\ Tv + \sin 2\varphi_c\ Th + \cos 2\varphi_c\ T3) - \\
& \mathrm{Im}(g_{vv}g_{hh}^{*} + g_{vh}g_{hv}^{*})\ T4 \qquad \text{(A4c)}
\end{aligned}
$$

$$
\begin{aligned}
T42 = \quad & 2\mathrm{Im}(g_{vv}\, g_{hv}^{*})\ (\cos^2\varphi_c\ Tv + \sin^2\varphi_c\ Th + 0.5\sin 2\varphi_c\ T3) + \\
& 2\mathrm{Im}(g_{hh}^{*}\, g_{vh})\ (\sin^2\varphi_c\ Tv + \cos^2\varphi_c\ Th - 0.5\sin\varphi_c\ T3) + \\
& \mathrm{Im}(g_{vv}g_{hh}^{*} + g_{vh}g_{hv}^{*})\ (-\sin 2\varphi_c\ Tv + \sin 2\varphi_c\ Th + \cos 2\varphi_c\ T3) + \\
& \mathrm{Re}(g_{vv}g_{hh}^{*} - g_{vh}g_{hv}^{*})\ T4 \qquad \text{(A4d)}
\end{aligned}
$$

In computing the general cases illustrated in Figures 8-9, the expressions given in Equations A4a-d were used in the special T3 = T4 = 0. That is, it is assumed that the 3rd and 4th Stokes parameters at the surface are zero.

# Appendix B

## Rotation Angles

I. Faraday Rotation

The rotation of the polarization vector of a linearly polarized plane wave propagating along the path S from [0,L] is (Le Vine and Abraham, 2002; Thompson, Moran, Swenson, 1986):

$$\Omega_F = (\pi/c\nu^2) \int_0^L \nu_p^2(s)\, \nu_B(s)\, \mathrm{Cos}(\Theta_B(s))\, ds \qquad \text{(B1)}$$

where $\nu$ is frequency, $\nu_p$ and $\nu_B$ are the plasma and gyro frequencies, respectively, and $\Theta_B$ is the angle between the propagation vector and magnetic field:

$$\Theta_B = \cos(\theta)\sin(I) - \sin(\theta)\cos(I)\cos(\varphi - D) \qquad \text{(B2)}$$

In the expression above, $(\theta,\varphi)$ are the polar coordinates of the line of sight from the spacecraft to the observation point on the surface, and (I,D) are the local magnetic "dip" angle and declination, respectively.

At L-band (1.4 GHz) Equation B1 can be simplified and, to a reasonable approximation, one obtains (Le Vine and Abraham, 2002):

$$\Omega_F \approx 6950\, B_{400}\, \mathrm{Cos}(\Theta_B)\, \sec(\theta_F)\, \mathrm{VTEC} \qquad \text{(B3)}$$

where $\theta_F$ is the angle between the propagation vector and nadir, $B_{400}$ the value of the magnetic field at 400 km and VTEC is the vertical total electron content.

In the calculations presented in this manuscript, the Faraday rotation angle, $\Omega_F$, has been obtained by applying Equation B3 using parameters above the midpoint of the propagation path between the surface and the spacecraft. $B_{400}$ and $\Theta_B$ are evaluated using the magnetic field at 400 km above this point and VTEC is the electron content in the vertical column above this point up to the altitude of the spacecraft. The TEC is computed using the IRI-2000 to model the ionosphere (Bilitza, 2001) and the magnetic field is obtained from the International Geomagnetic Reference Field (IGRF; Barton, 1997). In the examples presented here the ionosphere for November 14, 2004 was used for low solar activity and November 14, 2001 was used for high solar activity.

II. Geometrical Rotation

The angle $\varphi_c = \varphi + \Omega_F$ needed in the rotation matrix (Equation 6) consists of the Faraday rotation, $\Omega_F$, described above and an angle, $\varphi$, due to the fact that the polarization vectors (**h**,**v**) at an arbitrary point on the surface are not aligned with the definitions at the antenna.

For the antenna, the "Ludwig-3 definition (Equation 3) is used to define polarization (Ludwig, 1973). It is assumed that at the antenna boresight the "vertical" polarization port of the antenna is aligned with the conventional radiometric definition of vertical polarization at the surface. In the local antenna coordinate system (**x**,**y**,**z**), this direction is assigned to the x-axis and the z-axis is along boresight. With this definition, vertical polarization at boresight is aligned with $\boldsymbol{\varepsilon}_1$ as defined in Equation 3. Unfortunately, the Ludwig-3 definition uses the "radar" definition of polarization (i.e. looking away from the antenna) and in radiometry it is conventional to define **v** and **h** as if propagating away from the surface toward the antenna. The result is that at boresight the direction of horizontal polarization in the antenna reference frame, $\boldsymbol{\varepsilon}_2$, is now opposite to the direction of **h** at the surface ($\mathbf{h} \bullet \boldsymbol{\varepsilon}_2 = -1$ at boresight). This sign difference becomes an annoyance that must be keep in mind when dealing with antenna patterns which are usually delivered in conventional coordinates!

At points other than boresight, the antenna polarization is given by $\boldsymbol{\varepsilon}_1$ and $\boldsymbol{\varepsilon}_2$ as defined in Equation 3. These vectors are orthogonal, and orthogonal to the line-of-sight between the antenna and surface, but they are rotated with respect to the corresponding values at the surface:

$$\mathbf{v} \bullet \boldsymbol{\varepsilon}1 = \cos(\varphi)$$
$$\mathbf{h} \bullet \boldsymbol{\varepsilon}1 = -\sin(\varphi) \qquad \text{(B4)}$$

In Equation B4 $\varphi$ is the angle by the same name in Equation 3 and is the "azimuth" in a conventional spherical coordinate system centered on the local antenna coordinates (**x**,**y**,**z**). It is measured from the x-axis and is positive in the direction toward the positive y-axis in the antenna coordinate system.

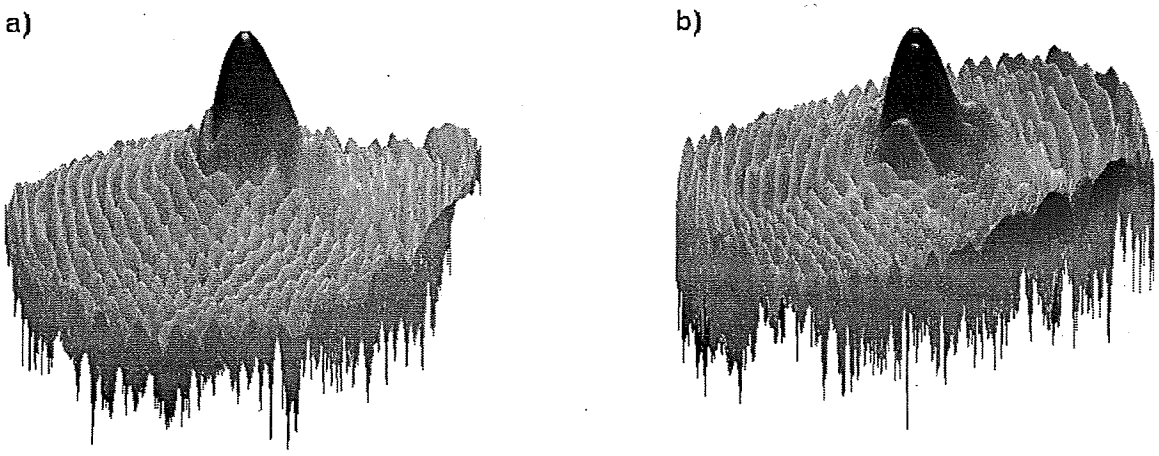


Figure 1. Example antenna patterns. Shown are (a) the co-polarized pattern and (b) the cross-polarized pattern for the horizontally polarized channel of the outer-most beam in the Aquarius radiometer. The peak level on the left (a) is about 25 db less than on the right (b).

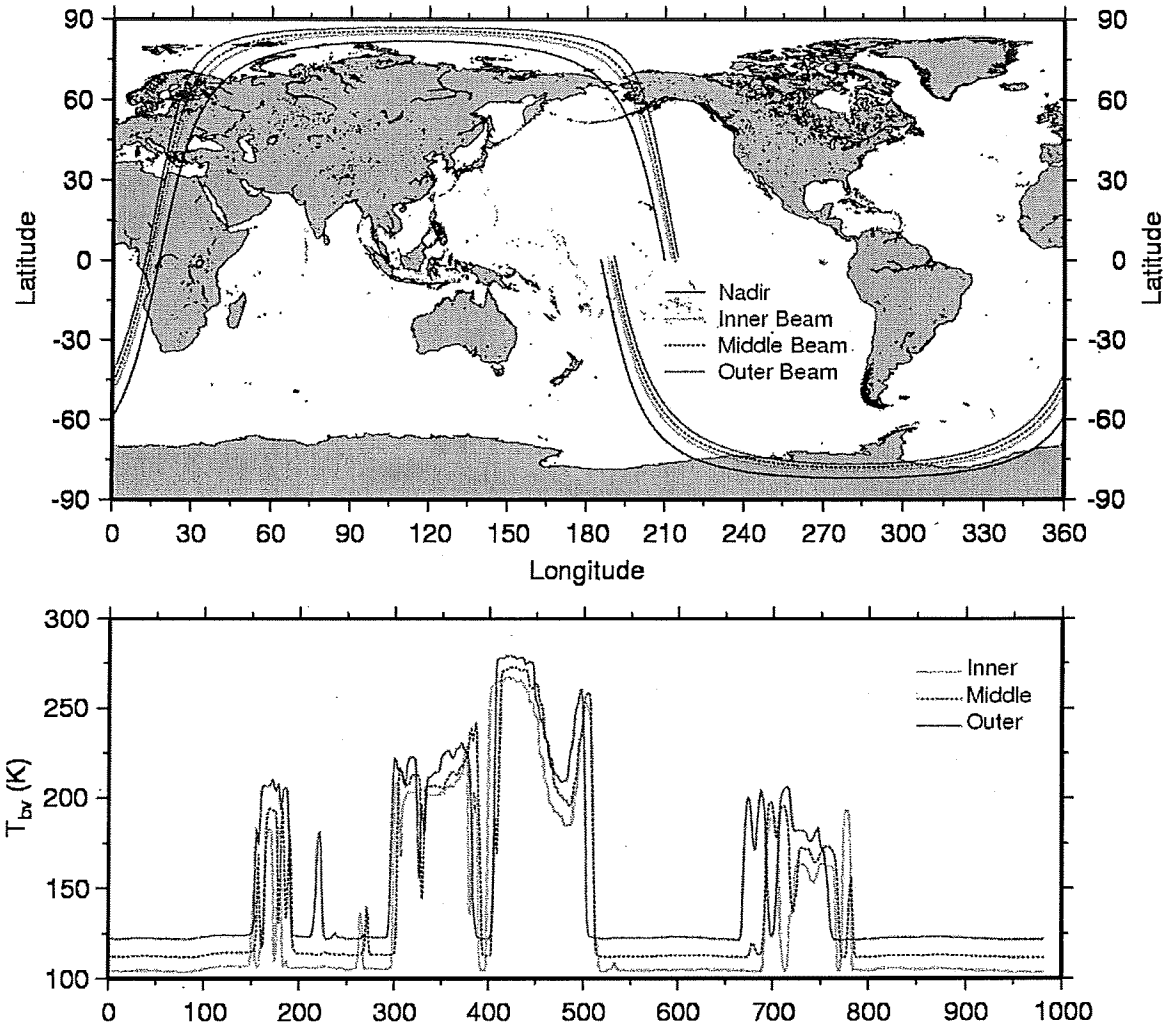


Figure 2. Top: Ground track (bold) and beam boresight for each of the three Aquarius radiometer beams during one orbit. Bottom: The brightness temperature at vertical polarization for the three beams during this orbit. The large jumps in level occur at the transitions from land to water. The different values over water reflect the different incidence angles of the three beams. The index on horizontal axis in the figure at the bottom indicates sample points in the calculations (one calculation every 6 seconds).

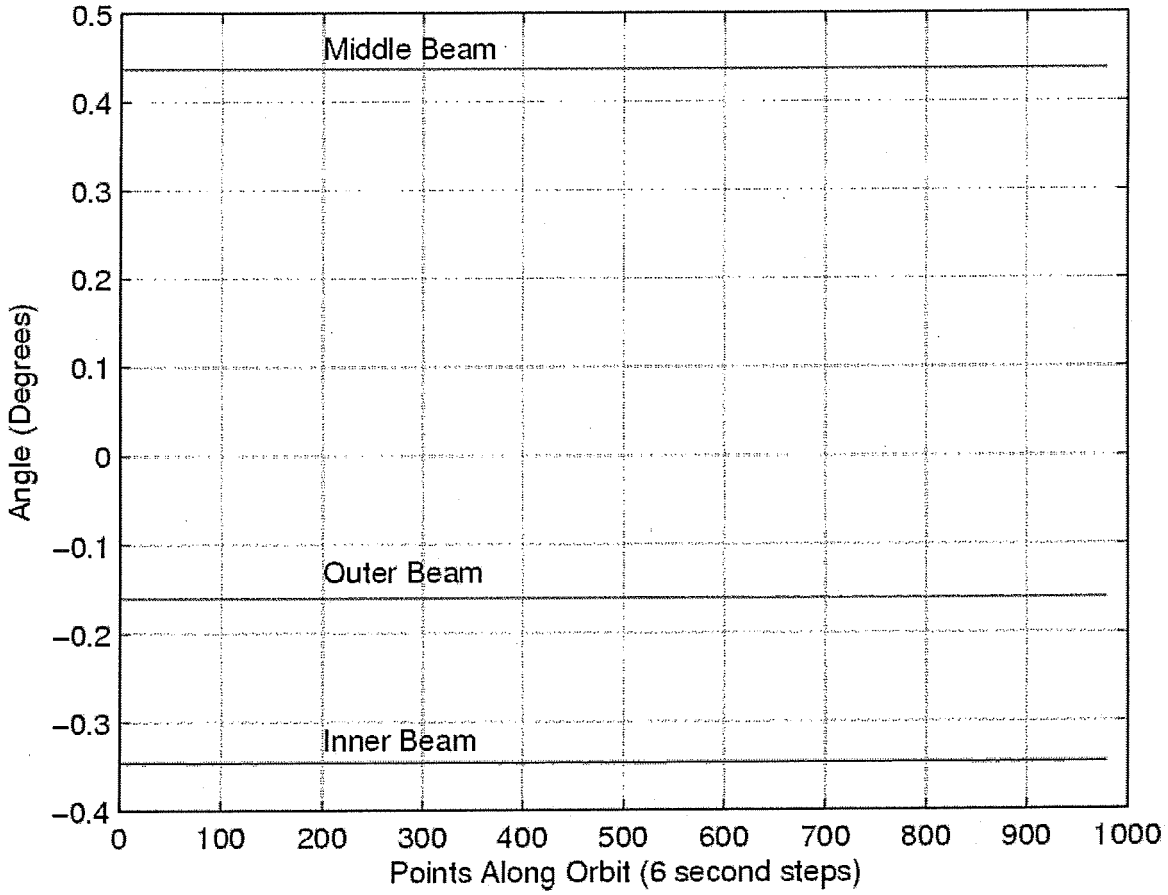


Figure 3: Retrieved angle in the ideal case (identical patterns with no cross-polarization) and no Faraday rotation. The angle is due to changes in geometry over the antenna footprint.

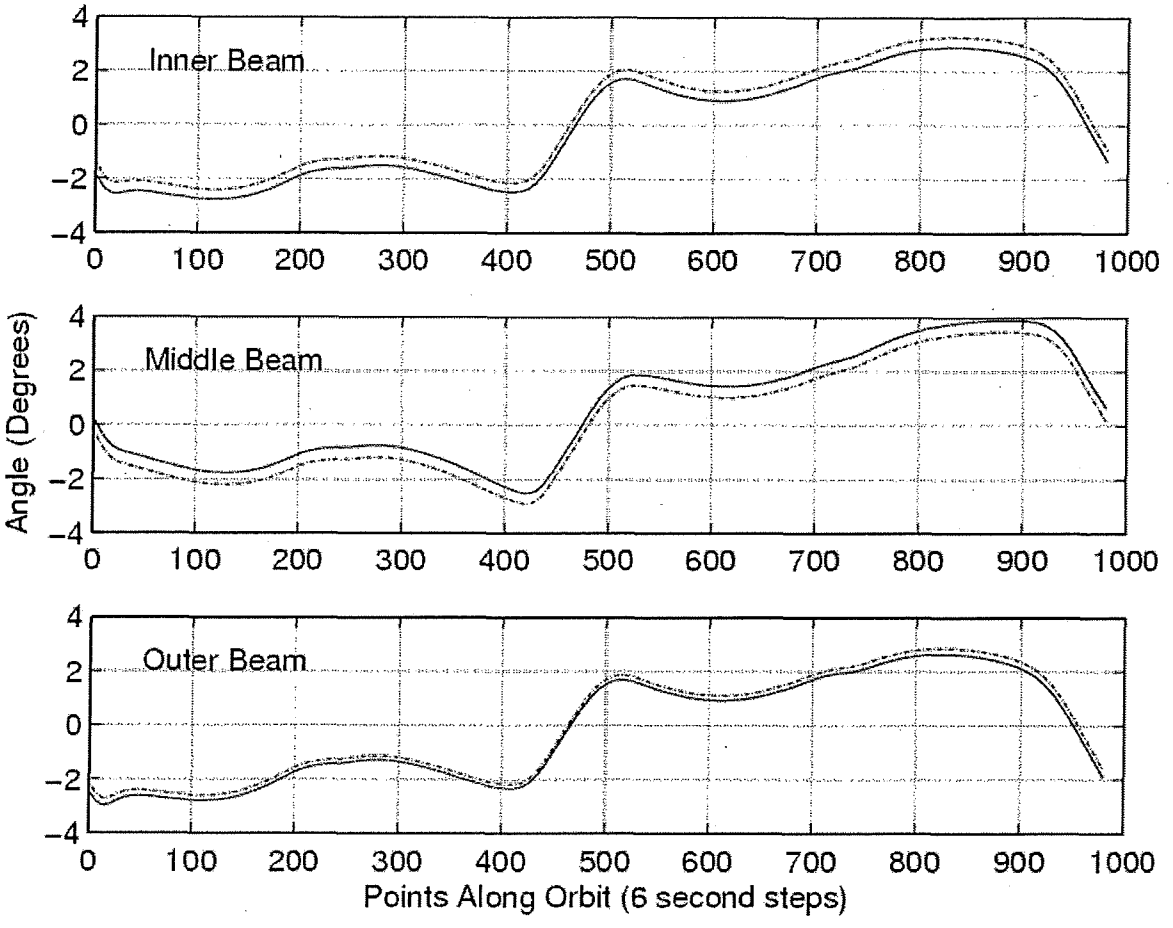


Figure 4. The retrieved angle during one orbit in the ideal case with Faraday rotation included. The dominant contribution is due to Faraday rotation. The dashed line is the value at boresight. The sign changes occurs at equatorial crossings (0 and 450) due to the change in the sign of the magnetic field "dip" angle.

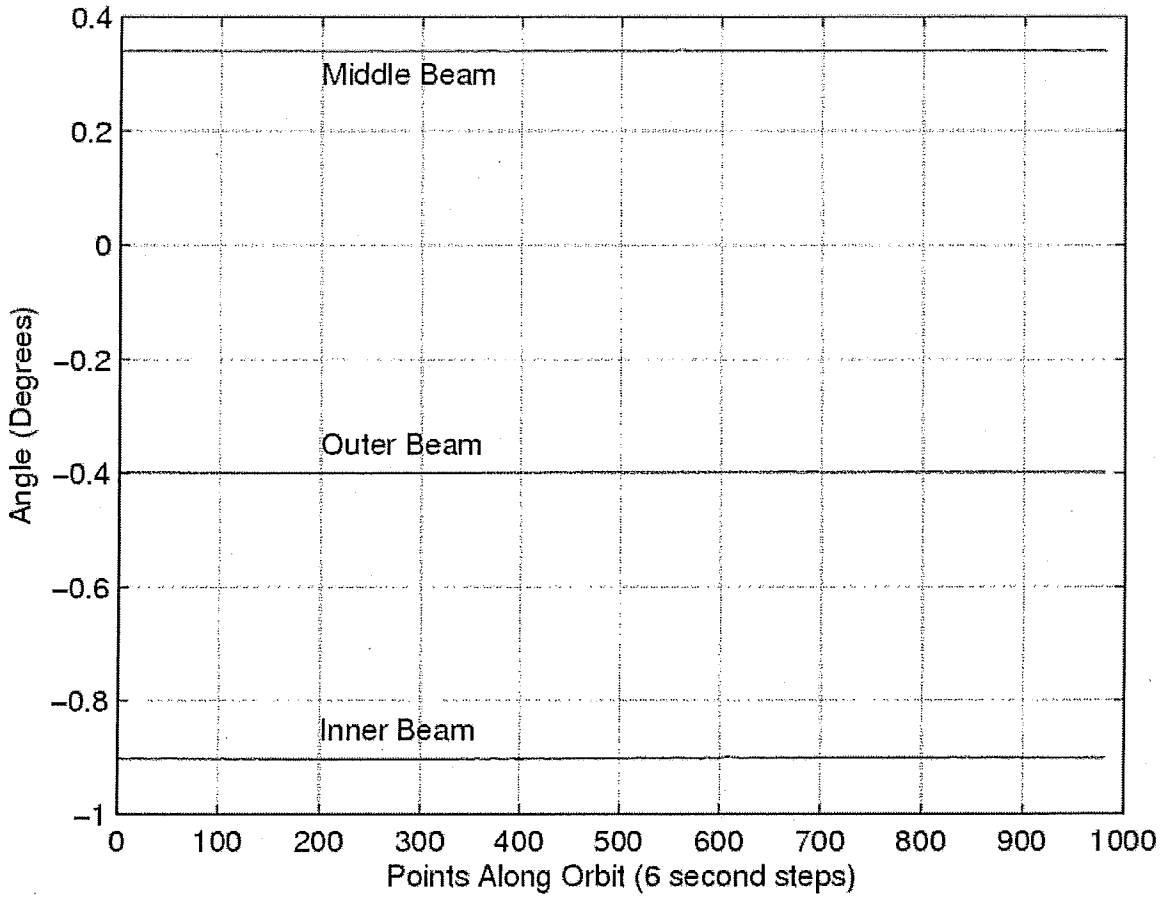


Figure 5. The effect of cross-polarization coupling on the retrieved angle. This is for the same case as in Figure 3, idealized pattern and no Faraday rotation, but with cross-polarization coupling included.

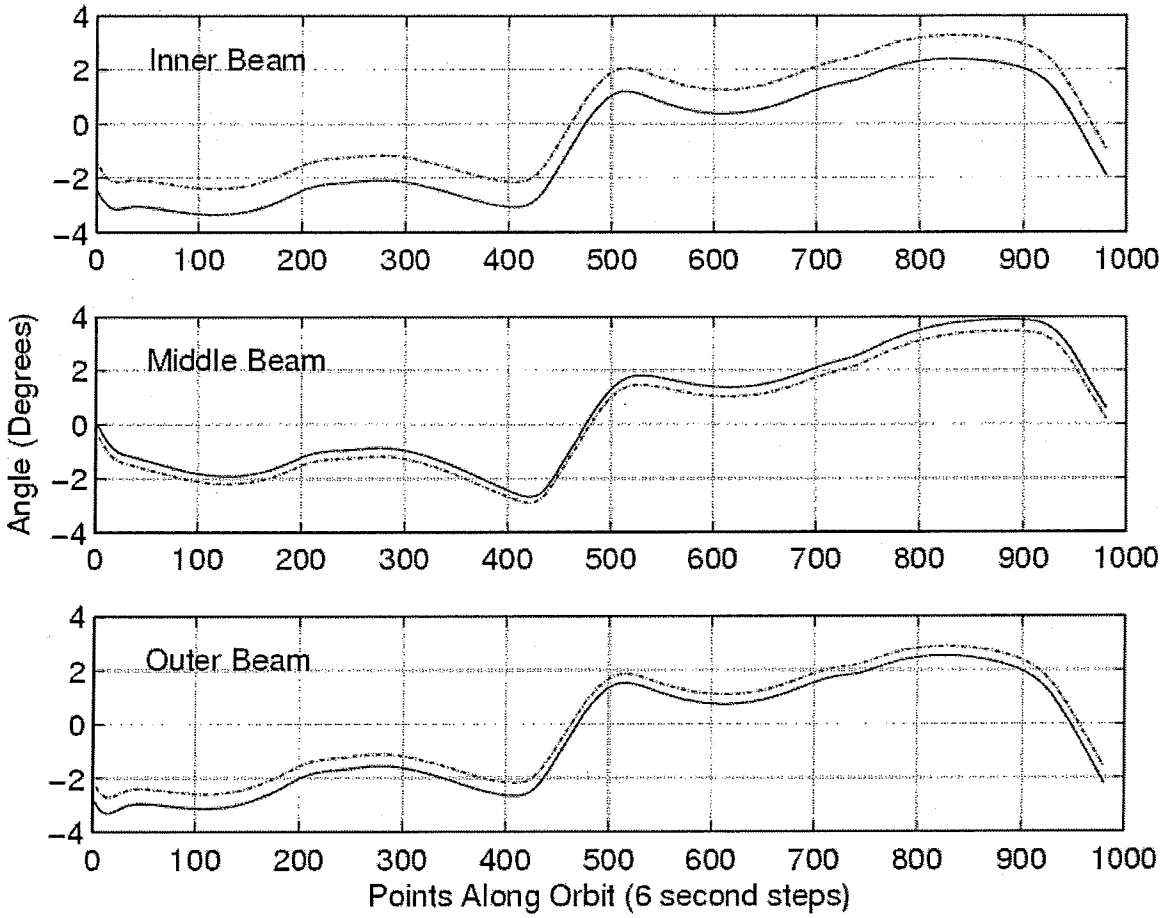


Figure 6. The effect of cross-polarization coupling on the retrieved Faraday rotation angle. The antenna patterns are the same as in the ideal case but with cross-polarization included. The dotted curve is the value retrieved at antenna boresight.

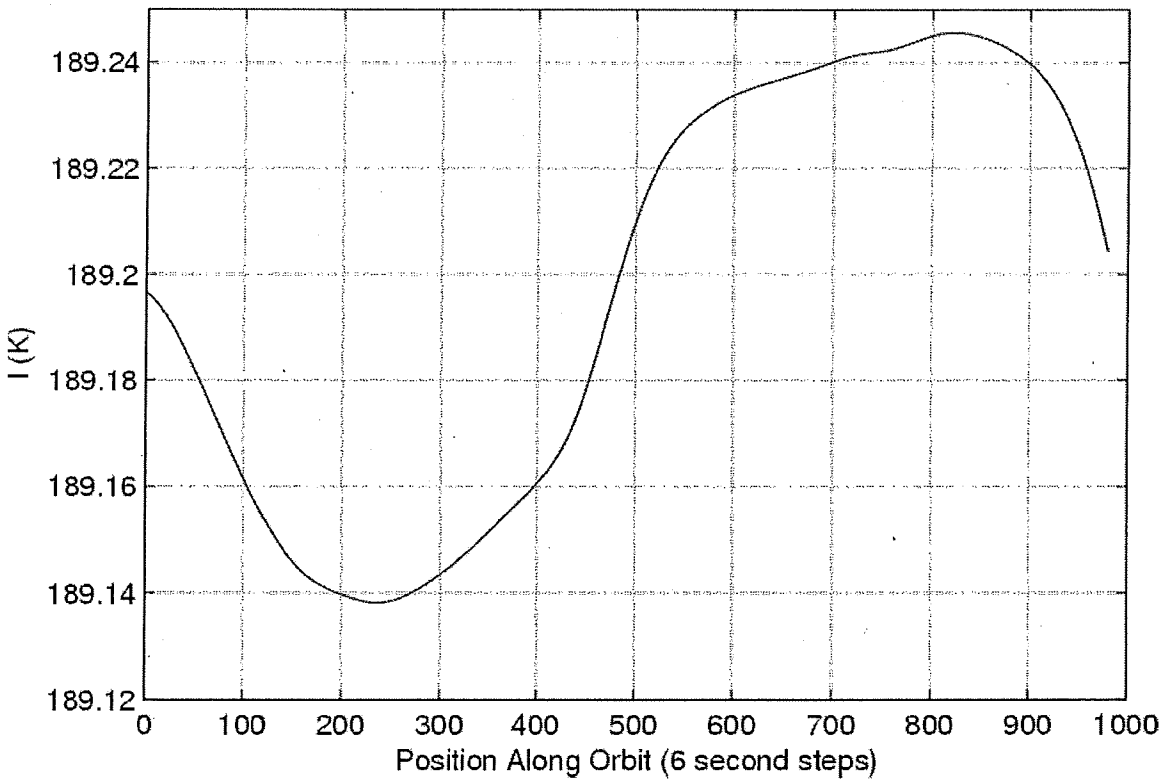


Figure 7. The effect of cross-polarization coupling on the first Stokes parameter, I = Tv + Th, in the special case defined by Equations 11. The example shown is for the outer beam.

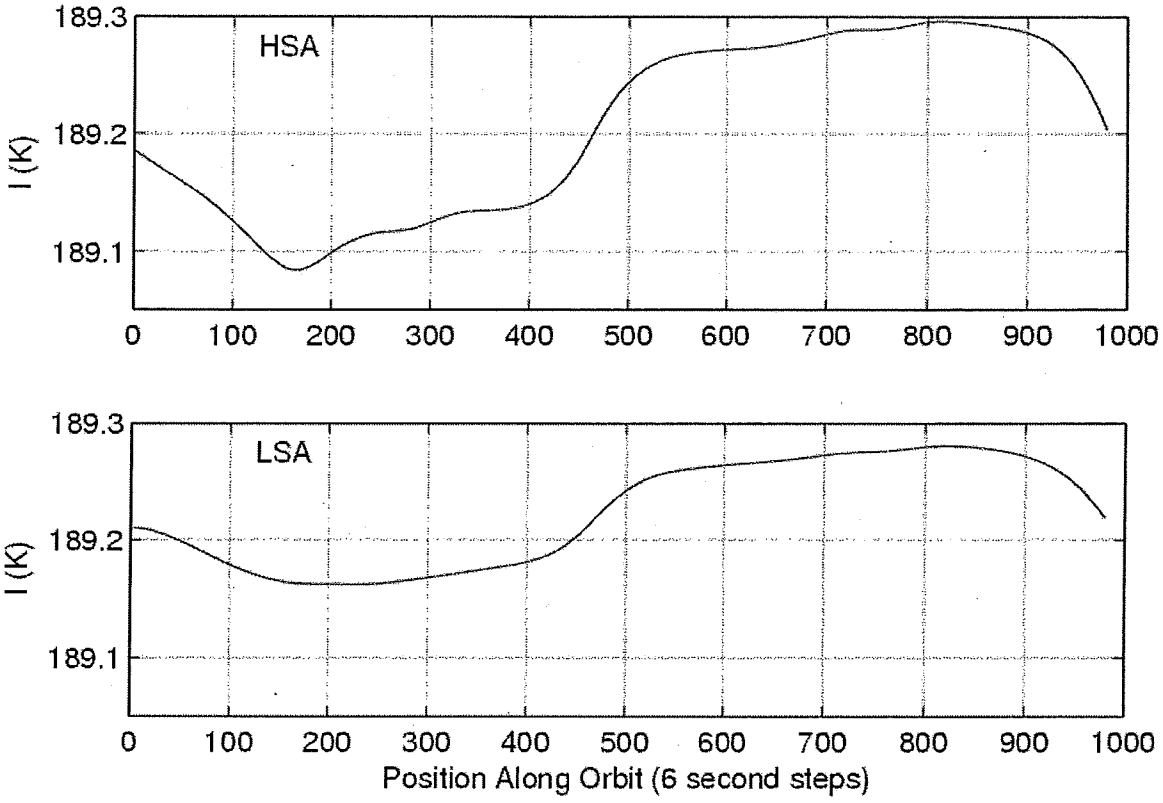


Figure 8. The effect of Faraday rotation on the first Stokes parameter, I = Tv + Th, in the general case using the complete Aquarius antenna patterns. The top panel is for high solar activity (HSA) and the lower panel for an ionosphere representative of low solar activity (LSA).

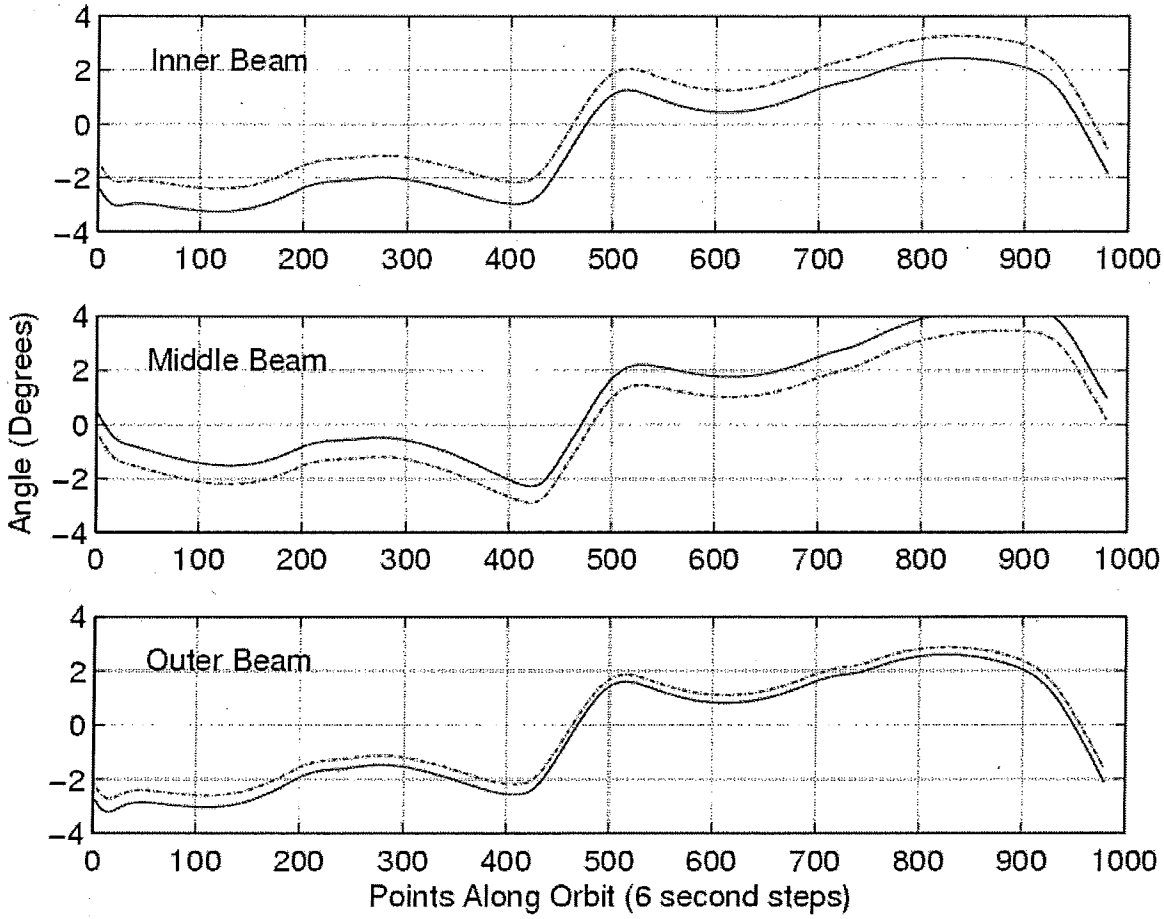


Figure 9a. The retrieved angle in the general case using the actual Aquarius antenna patterns. The dotted line is the value at the antenna boresight where there is no geometrical bias. This example is for a case of low solar activity.

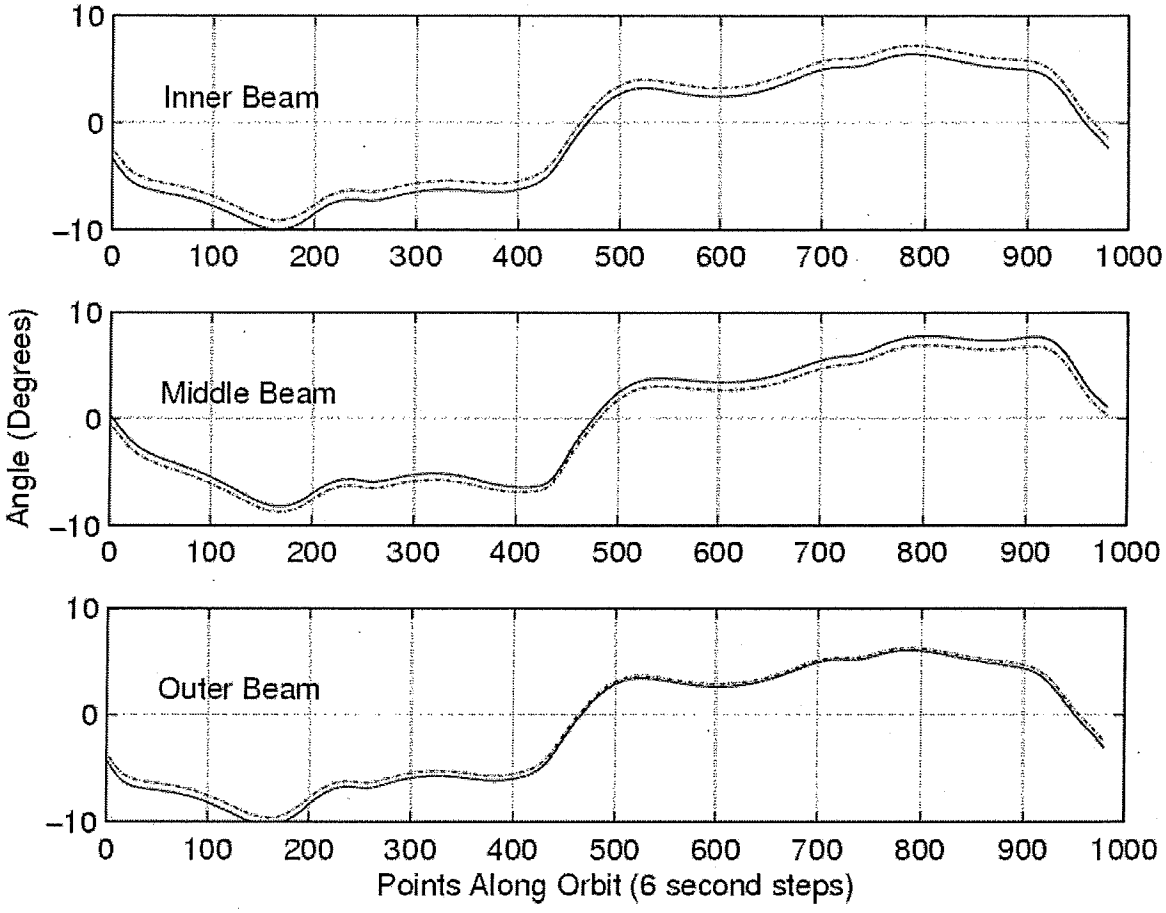


Figure 9b. The retrieved angle in the general case using the actual Aquarius antenna patterns. The dotted line is the value at the antenna boresight where there is no geometrical bias. This example is for a case of high solar activity. The results are similar to those shown in Figure 9a (low solar activity) but the dynamic range is about 2.5 times larger.